Copy No._____

Defence Research and Development Canada
Recherche et développement pour la défense Canada

DEFENCE R&D DÉFENSE

Validation of TRANSOM

T. Chisholm

D. W. Zingg
University of Toronto

University of Toronto
Institute of Aerospace Studies
4925 Dufferin Street
Toronto, ON
M3H 5T6

Project Manager: L. Gilroy, 902-426-3100 ext. 365

Contract Number: W7707-01-1110

Contract Scientific Authority: D. Hally, 920-426-3100 ext. 212

Defence R&D Canada – Atlantic

Contract Report
DRDC Atlantic CR 2004-229
October 2004

Canada

Validation of TRANSOM

T. Chisholm

D.W. Zingg
University of Toronto, Institute of Aerospace Studies

University of Toronto, Institute of Aerospace Studies
4925 Dufferin St., Toronto, ON, M3H 5T6

Project Manager: L. Gilroy 902-426-3100 Ext. 365

Contract Number: W7707-1-1110

Contract Scientific Authority: D. Hally 902-426-3100 Ext. 212

Defence R&D Canada – Atlantic

Contract Report

DRDC Atlantic CR 2004-229

October 2004

Approved by

R. Kuwahara
Head/Signatures

Approved for release by

K. Foster
Chair/Document Review Panel

The scientific or technical validity of this Contractor Report is entirely the responsibility of the contractor and the contents do not necessarily have the approval or endorsement of Defence R&D Canada.

© Her Majesty the Queen as represented by the Minister of National Defence, 2004
© Sa majesté la reine, représentée par le ministre de la Défense nationale, 2004

106-03820/

Abstract

A series of test cases, including a two-dimensional airfoil, flow over a prolate spheroid, and the Wigley, Dyne, and Kriso hulls, was used to validate TRANSOM, a flow solver developed at DRDC Atlantic. TRANSOM is quite sensitive to the quality of the grid. Suitable grids can be difficult to produce with the tools available. The results suggest changes to the boundary conditions to improve accuracy without requiring further restrictions on grid generation. Accurate results are obtained for most of the test cases.

Résumé

Une série de tests élémentaires, portant notamment sur l'écoulement le long d'une surface portante à deux dimensions, d'un sphéroïde allongé et des carènes de Wigley, de Dyne et de la KRISO, a été utilisée pour valider TRANSOM, un résolveur de problèmes liés à l'écoulement développé par RDDC Atlantique. TRANSOM est très sensible à la qualité du maillage. Des maillages convenables peuvent être difficiles à produire avec les outils disponibles. Les résultats des essais indiquent quelles modifications doivent être apportées aux conditions limites pour améliorer l'exactitude sans restrictions additionnelles lors de la création du maillage. Des résultats exacts sont obtenus pour la plupart des test élémentaires.

This page intentionally left blank.

Executive summary

Background

The flow into a propeller significantly affects both its efficiency and the extent to which it cavitates. Therefore, to design an effective propeller, it is necessary to know, in advance, what the flow through the propeller will be. DRDC Atlantic has developed the flow solver TRANSOM for this purpose. This purpose of the current work was to determine how effective TRANSOM is at calculating the flows around ships.

Principal results

A series of test cases, including a two-dimensional airfoil, flow over a prolate spheroid, and the Wigley, Dyne, and Kriso hulls, was used to validate TRANSOM. TRANSOM is quite sensitive to the quality of the grid. Suitable grids can be diffcult to produce with the tools available. The results suggest changes to the boundary conditions to improve accuracy without requiring further restrictions on grid generation. Accurate results are obtained for most of the test cases.

Significance of results

The results of this study show that TRANSOM is a useful tool for predicting the flow around hulls and into the propeller plane. It can be used to facilitate the design and analysis of low-noise propellers.

Future work

Work needs to be done to improve the boundary conditions to decrease the sensitivity of the results to the grids used.

T. Chisholm, D.W. Zingg; 2004; Validation of TRANSOM;
DRDC Atlantic CR 2004-229; Defence R&D Canada – Atlantic.

Sommaire

Introduction

L'écoulement dans une hélice a une très grande incidence sur l'efficacité de cette dernière et sur l'importance de la cavitation qu'elle produit. En conséquence, pour concevoir une hélice efficace, il est nécessaire de connaître à l'avance les caractéristiques de l'écoulement à travers l'hélice. À cette fin, RDDC Atlantique a développé TRANSOM, un résolveur de problèmes liés à l'écoulement. La présente étude a pour objet de déterminer si TRANSOM pouvait efficacement calculer les écoulements autour de navires.

Principaux résultats

Une série de tests élémentaires, portant notamment sur l'écoulement le long d'une surface portante à deux dimensions, d'un sphéroïde allongé et des carènes de Wigley, de Dyne et de la KRISO, a été utilisée pour valider TRANSOM. TRANSOM est très sensible à la qualité du maillage. Des maillages convenables peuvent être difficiles à produire avec les outils disponibles. Les résultats des essais indiquent quelles modifications doivent être apportées aux conditions limites pour améliorer l'exactitude sans restrictions additionnelles lors de la création du maillage. Des résultats exacts sont obtenus pour la plupart des test élémentaires.

Portée des résultats

Les résultats de cette étude montrent que TRANSOM est un outil pratique pour la prédiction des écoulements autour des coques et dans le plan de l'hélice et qu'il peut s'avérer utile pour la conception et l'analyse des hélices silencieuses.

Recherches futures

Il y a encore du travail à faire pour améliorer les conditions limites de manière à diminuer la vulnérabilité des résultats aux maillages utilisées.

T. Chisholm, D.W. Zingg; 2004; Validation of TRANSOM;
DRDC Atlantic CR 2004-229; R & D pour la défense Canada – Atlantique.

Table of contents

Abstract i

Résumé i

Executive summary iii

Sommaire iv

Table of contents v

List of figures vi

1 Introduction 1

2 Grid Generation 2

3 Convergence 5

4 Test cases 6

4.1 NACA 0012 Airfoil 6

4.2 Spheroid 8

4.3 Hulls 17

4.3.1 Wigley Hull 18

4.3.2 Dyne Hull 24

4.3.3 Kriso KCS Hull 33

5 Conclusions 40

References 41

List of figures

1	Modification of control functions	4
2	Pressure around NACA 0012 airfoil	6
3	Pressure distribution on NACA 0012	7
4	Spheroid grid	9
5	Flow over spheroid	10
6	Boundary layer on spheroid $z = -0.02$	11
7	Pressure distribution on spheroid	12
8	Spheroid slice $z = -0.02$, 15 chord boundary	13
9	Boundary layer on spheroid $z = -0.02$ with extended boundary	14
10	Boundary layer on spheroid $z = 0.14$ with extended boundary	15
11	Pressure distribution on spheroid with extended boundary	16
12	Grid around Wigley hull	18
13	Grid on body of Wigley hull	19
14	Streamwise velocity on Wigley hull $x = 0.5$	21
15	Streamwise velocity on Wigley hull $x = 0.9$	21
16	Streamwise velocity on Wigley hull $x = 1.0$	22
17	Streamwise velocity on Wigley hull $x = 0.5$, with fine symmetry	22
18	Streamwise velocity on Wigley hull $x = 0.9$, with fine symmetry	23
19	Streamwise velocity on Wigley hull $x = 1.0$, with fine symmetry	23
20	Dyne tail	25
21	Dyne hull	26
22	Effect of refined symmetry	26

23 Streamwise velocity on Dyne hull, $x = 0.646$ 27
24 Streamwise velocity on Dyne hull, $x = 0.921$ 27
25 Streamwise velocity on Dyne hull, $x = 0.989$ 28
26 Streamwise velocity on Dyne hull, $x = 1.018$ 28
27 Cross-flow velocities on Dyne hull, x=0.921 29
28 Cross-flow velocities on Dyne hull, x=1.018 30
29 Pressure on Dyne hull, $x = 0.645$ 31
30 Pressure on Dyne hull, $x = 0.917$ 31
31 Pressure on Dyne hull, $x = 0.964$ 32
32 Kriso hull 33
33 Kriso body grid detail 34
34 Kriso hull velocities at station 2 35
35 Kriso hull velocities at station 1 36
36 Kriso hull velocities at station 0.35 37
37 Kriso hull velocities at station -0.5767 38
38 Kriso hull velocities at station -2 39

1 Introduction

A multi-year effort to develop a Navier-Stokes solver for modeling flow around ship hulls, over appendages and control surfaces, and through propellers is underway at Defence R&D Canada – Atlantic (DRDC – Atlantic). Previous contracts with the University of Toronto have developed software for generating grids about a range of three-dimensional hull geometries [1], for the numerical solution of the steady, laminar, incompressible Navier-Stokes equations in two and three dimensions [2, 3], and improvements of the former to solve turbulent flows [4], to be more general, and to increase performance and accuracy [5]. The two-dimensional flow solver NSI2D was modified at DRDC in 1994, and incorporated into the multi-method code TRANSOM [6]. The ability to use multiple-block grids was added to TRANSOM [7]. This included the option to have discontinuous metrics at the block boundaries [8]. TRANSOM will also handle rotating flows [9].

TRANSOM solves the pseudo-compressible form of the incompressible Navier-Stokes equations [10, 11, 12]. The spatial discretization is accomplished using a third-order upwind scheme based on flux-difference splitting [13]. Iteration to steady state is achieved using an approximate-Newton method based on an approximate Jacobian matrix which corresponds to the linearization of a first-order spatial discretization [14]. The resulting linear system is solved using the generalized minimal residual method (GMRES) of Saad and Schultz [15]. GMRES requires reasonably tight clustering of the eigenvalues of the matrix in order to converge in few iterations. To help cluster the eigenvalues, an incomplete LU preconditioner with an adjustable degree of fill is used. The Spalart-Allmaras turbulence model [16] is used to provide the turbulent viscosity for high Reynolds number flows.

The objective of the work was to determine the level of accuracy of TRANSOM as well as the strengths and weaknesses of the program. The test cases given are, for the most part, commonly used for similar studies. However the data, for the ship hulls in particular, is quite difficult to interpret and hard to come by. The results from the Wigley hull have been extracted from images given in a PhD thesis. The format used to describe the shape of the Dyne hull is particularly difficult to use. This required significant effort to grid.

2 Grid Generation

The grid quality was very important in this study. Grids of poor quality can introduce errors and cause serious difficulties in convergence. For this reason, a large proportion of the time was spent to ensure that quality grids were created. The grid generator previously developed, gem3d, was used and extended to generate most of the grids. Commercial codes were also used (such as GridGen and ICEM), but these had serious deficiencies compared to gem3d. For example GridGen seemed to have bugs which manifested when very small off-wall spacings (required for the turbulence model) were used. It is difficult to preserve grid orthogonality at the solid boundaries in certain regions. ICEM lacked the necessary smoothing abilities, and was in general extremely poorly documented and difficult to use.

Unfortunately, gem3d is also extremely difficult to use, although it provides excellent elliptic smoothing abilities, and the option to modify it as needed. A wrapper library was created in C++ to address some of the shortcomings. While this makes grid generation much easier, it is far from exhaustively tested and should be used with care.

Specific considerations for the grids for each case are discussed in the respective backgrounds. Here, we discuss the general approach taken to create the grids. The Reynolds number of the flow for all the three-dimensional cases is roughly the same, so that a common non-dimensional off-wall spacing of $5 \cdot 10^{-6}$ was used, based on the ship length as the reference distance. This gave $y^+ \approx 1.0$ at the first off-wall node, the value suggested by Spalart and Allmaras for their turbulence model. Note that the wrapper program uses absolute spacings, instead of a ratio of the spacing to the line length. This approach is much more intuitive, in most cases.

In order to provide enough nodes in the boundary layer, the spacing decay function control parameter at the solid boundaries was decreased from the default of 0.1 to 0.01. Decreasing this parameter increases the influence of the source function further into the grid. This also avoids problems with negative Jacobians of the metrics of the curvilinear transformation. Unfortunately, the 'floating boundary' feature of gem3d appears to be broken. The boundaries perpendicular to these solid boundaries would normally be set to float, so that the node distribution there would match the off-wall distribution in the interior. This is generally not a problem for the grids used here, though, since these boundaries are typically far removed from the rapidly changing regions of flow.

Only the parameter controlling the off-boundary spacing distribution is modi-

fied from the default. There is also the option to change the parameter controlling the off-boundary orthogonality. There is no need to adjust this parameter at boundaries with small off-boundary spacing, but it may be decreased (which increases the influence further into the grid) at boundaries with large spacings. This helps ensure orthogonality at the boundary.

Ensuring convergence of the elliptic solver is very difficult. There are a number of controls to help, but it is not easy to determine which to adjust. There is the option to set the relaxation parameter of the SOR solver, relaxation and damping rates of the control source functions on the boundaries, as well as the ability to zero these functions at specified regions. The latter is often useful where the boundary makes a sharp turn. Zeroing the control functions at the nodes before and after the turn seems to aid convergence, and gives a smoother grid in the region near the turn. The disadvantage is that these nodes are no longer orthogonal. Figure 1 shows a simple example at the leading edge of an airfoil. The node right at the turn should not have the control function zeroed. There is no problem with achieving orthogonality here, and the spacing control tends to pull the next off-boundary node into the bend, minimizing the spacing here. Of course, the spacing in the spanwise direction should be minimized here as well to minimize error. Unfortunately, gem3d does not have control over the spacing *rates* on the boundary lines. This would require a one-dimensional elliptic smoother.

It is difficult to optimally set the SOR relaxation and damping and relaxation factors for the boundary control functions. Generally, smaller factors will give more stable results. However, due to the way the boundary control functions are implemented, the residual can drop to a point where it appears converged if the damping and relaxation factors are small. A large number of iterations (on the order of thousands) may be required in order to begin enforcing the boundary controls.

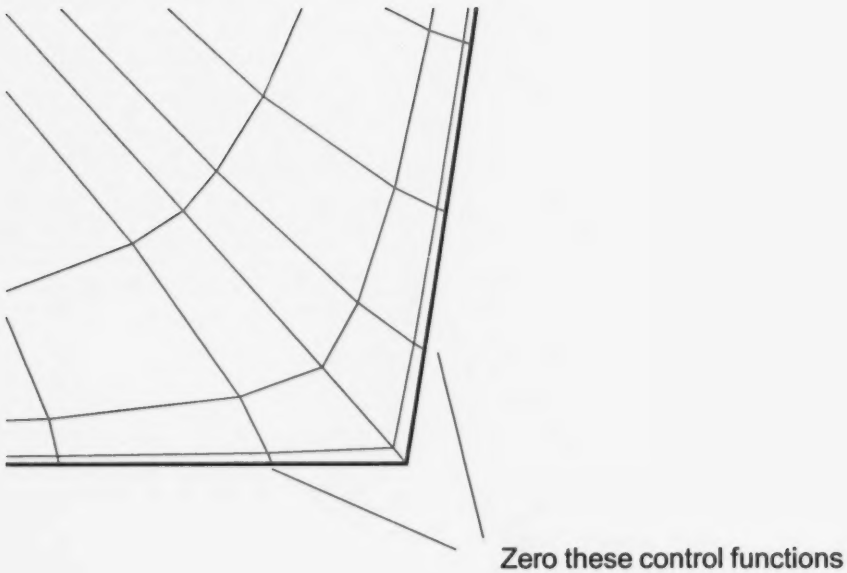

Figure 1: *Modification of control functions*

3 Convergence

The focus of this study is the on the quality of the results. The convergence histories are not presented. Generally, the three-dimensional cases were solved in two stages, the first with a lower time step for a number of iterations, until a higher time step is usable. Convergence is achieved when the maximum absolute residual (L_∞ norm) is less than 10^{-6}. Ideally, this number would be lower, but with the large grid sizes used, further convergence is quite time consuming. Also, the solution does not change significantly past this point.

***Figure 2:** Pressure around NACA 0012 airfoil*

4 Test cases

4.1 NACA 0012 Airfoil

The NACA 0012 airfoil was used as a simple two-dimensional test case. The grid was generated with the elliptical solver Amber2D. The C-grid has 305 nodes in the streamwise direction, and 57 in the off-wall direction. The off-wall spacing is 10^{-6}. The flow Reynolds number was 10^6, with an angle of attack of 6°.

Figure 2 shows the pressure coefficient around the airfoil. Figure 3 compares the pressure distribution on the surface of the airfoil with the well-validated solver, Scirocco [17]. No transition terms were used. The results compare favorably.

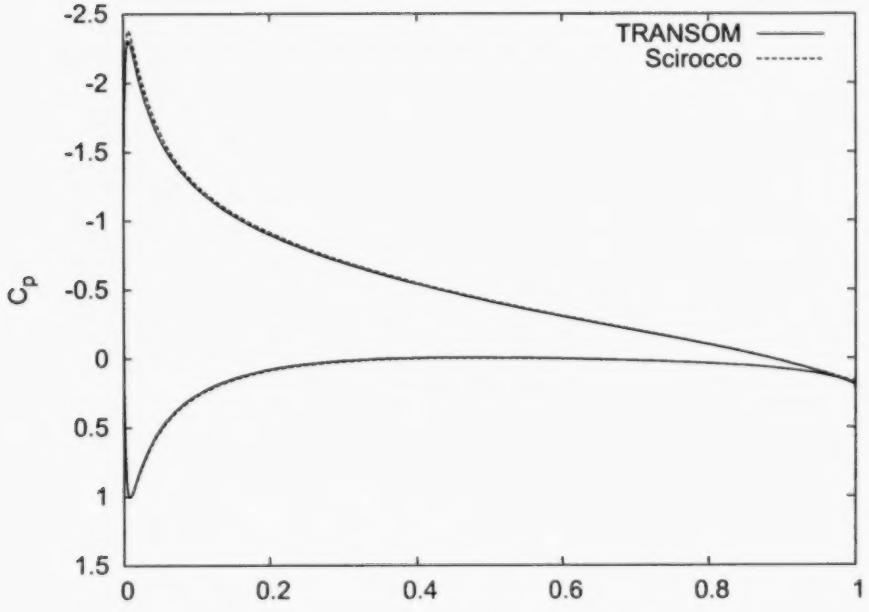

Figure 3: *Pressure distribution on NACA 0012*

4.2 Spheroid

The flow over a prolate spheroid has a number of excellent experimental data sets [18] [19] [20] [21], and so has been popular for validation of CFD results [22]. Here we have used the data set produced by Kreplin [21], who has kindly provided an electronic copy. The 10° angle of attack case was used. This case had a Mach number of 0.16 and a Reynolds number of $7.7 \cdot 10^6$. A transition strip was used at a non-dimensional length of $z = -0.3$, and there is a mild separation.

The geometry and grid generation are quite simple. Figures 4 and 5 show the grid used. Due to symmetry of the flow, a half-grid was appropriate. A line of degenerate cells was formed from either end. The grid was clustered around these lines to reduce the error induced from the 'axis' boundary condition. Grid size was 100 in the off-wall (ξ) direction, 50 in the azimuthal (η) direction, and 100 along the length (ζ). The original far-field distance was 15 chords. This was later increased to 40 for reasons demonstrated below. The freestream boundary condition was used at the far-field, except at the two points with degenerate cells. Here, either inflow or outflow was specified.

Figure 6 shows the experimental and numerical boundary layer on the spheroid at $z = -0.02$, at a number of angles around the body. Both the velocity and the length scales are non-dimensionalized by the free-stream velocity and body length. The origin is located at the centre of the body. Figure 7 shows the surface pressure distribution on a number of strips along the length of the body. There is clearly a large error, especially evident in Figure 6(a), where the edge of the boundary layer has a velocity 10% higher than experiment. An examination of the far-field (Figure 8) shows that an overly high velocity persists through to the boundary, especially near the portion which is inflow. Increasing the distance to the far-field to 40 improved results. Figures 9, 10, and 11 show the results with the extended boundary. They are much improved.

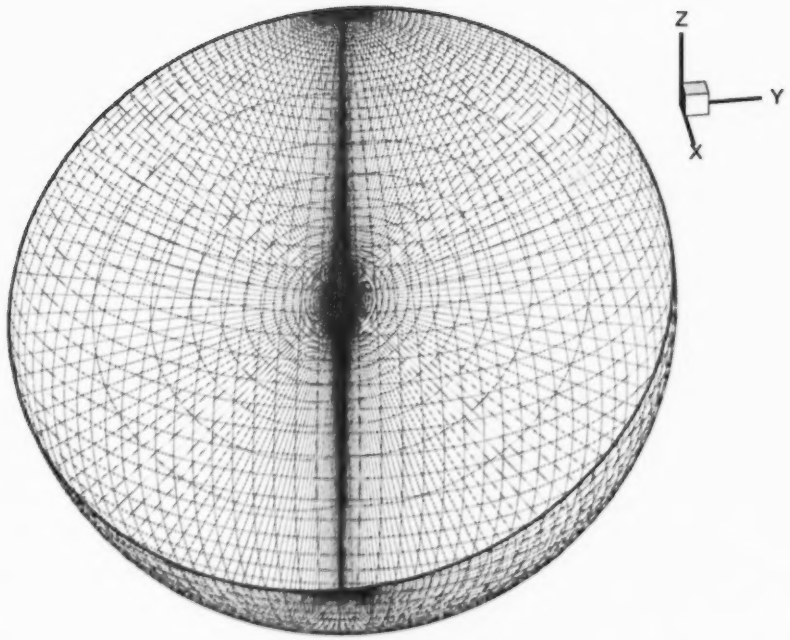

Figure 4: *Spheroid grid*

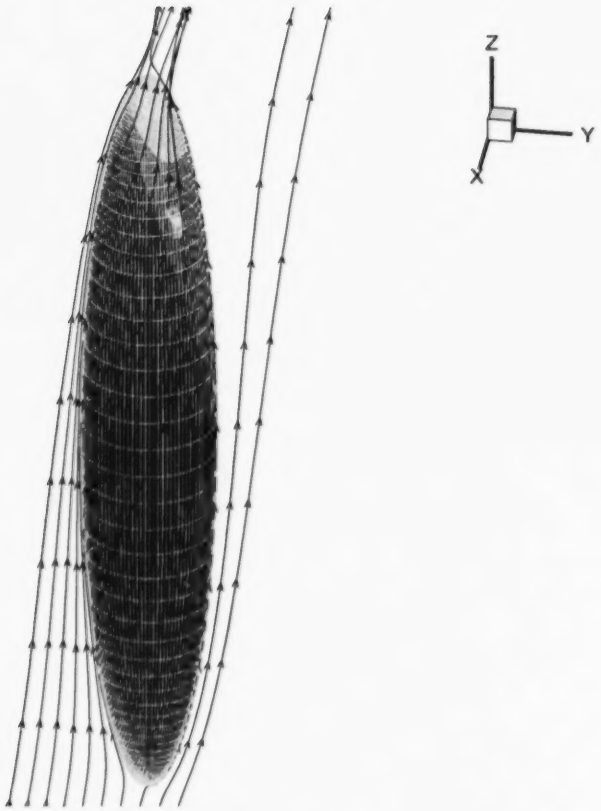

Figure 5: *Flow over spheroid*

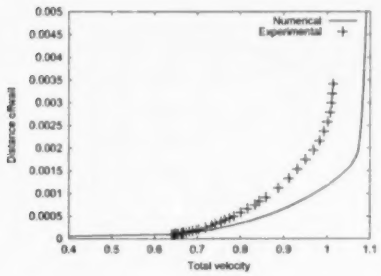

(a) 0°

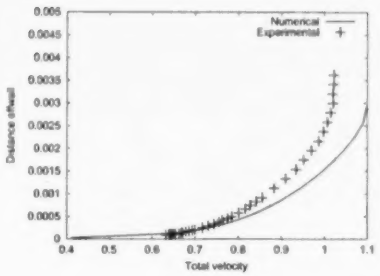

(b) 30°

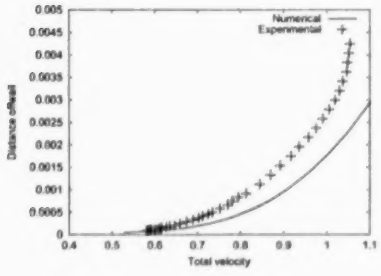

(c) 90°

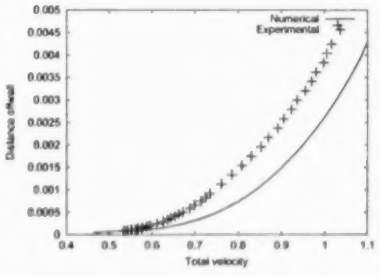

(d) 120°

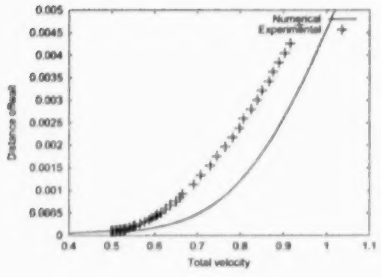

(e) 150°

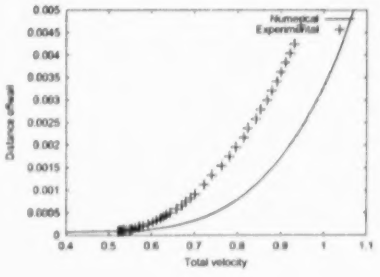

(f) 180°

Figure 6: *Boundary layer on spheroid* $z = -0.02$

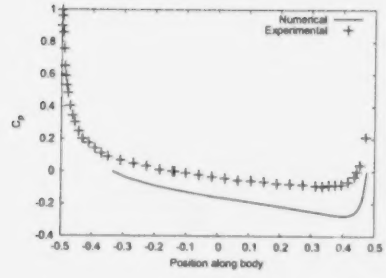

(a) 0°

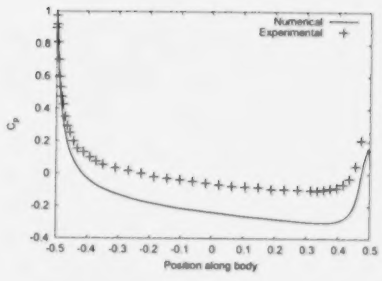

(b) 30°

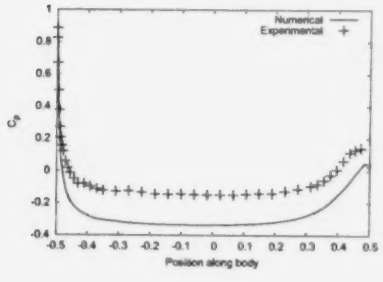

(c) 90°

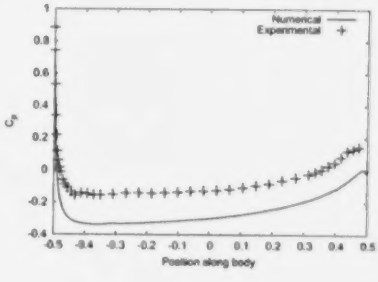

(d) 120°

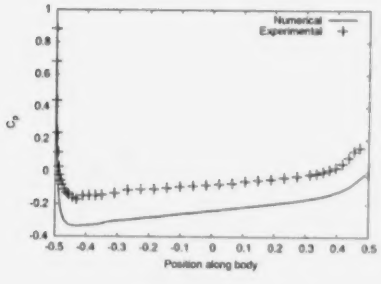

(e) 150°

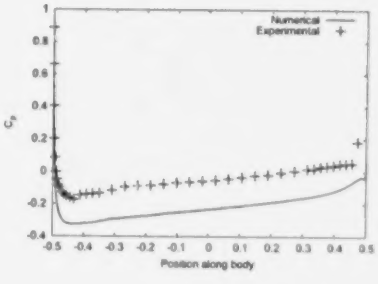

(f) 180°

Figure 7: *Pressure distribution on spheroid*

Figure 8: *Spheroid slice* $z = -0.02$*, 15 chord boundary*

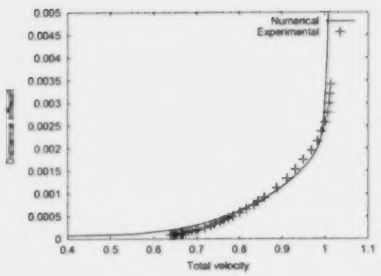

(a) 0°

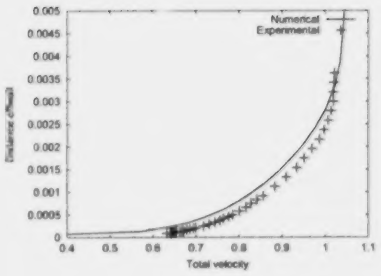

(b) 30°

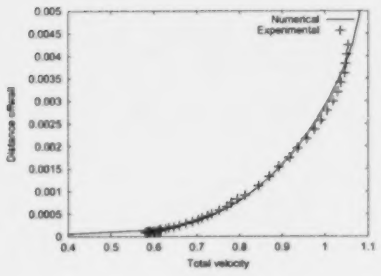

(c) 90°

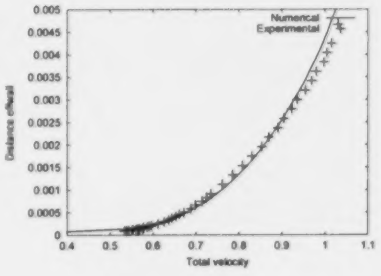

(d) 120°

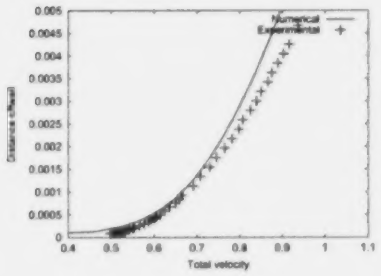

(e) 150°

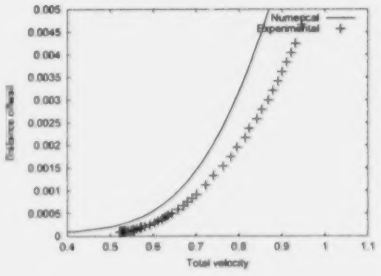

(f) 180°

Figure 9: *Boundary layer on spheroid* $z = -0.02$ *with extended boundary*

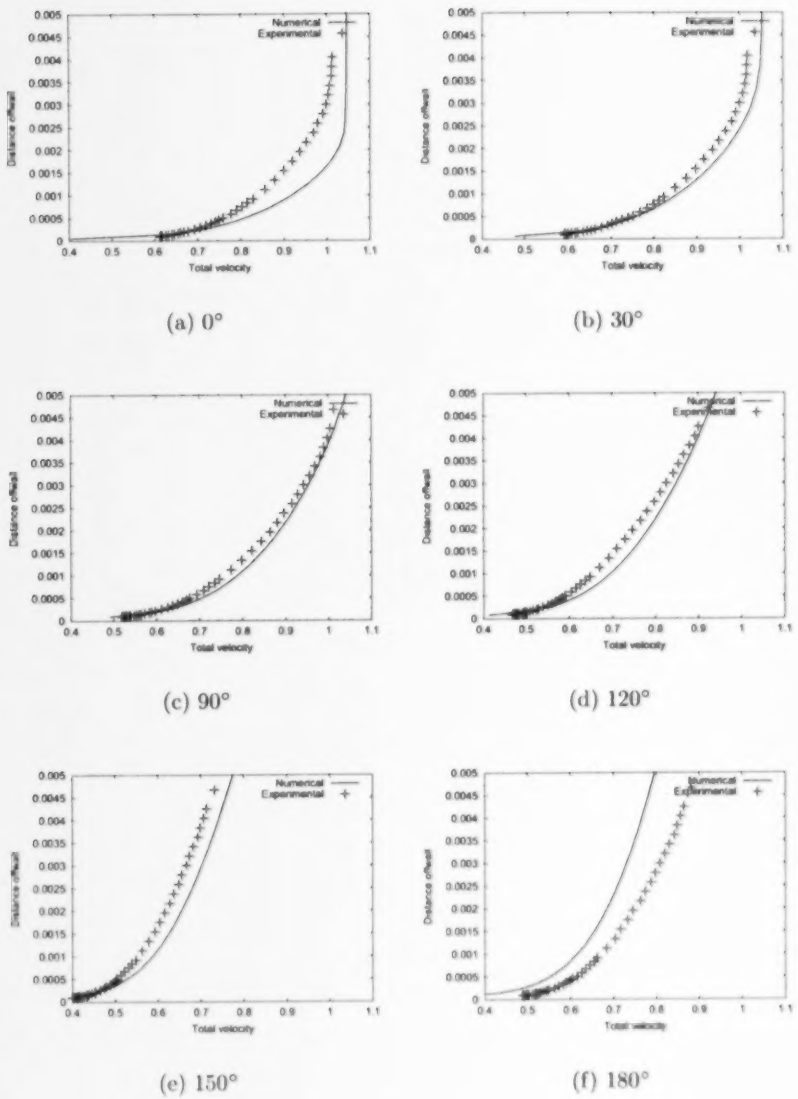

(a) 0°

(b) 30°

(c) 90°

(d) 120°

(e) 150°

(f) 180°

Figure 10: *Boundary layer on spheroid* $z = 0.14$ *with extended boundary*

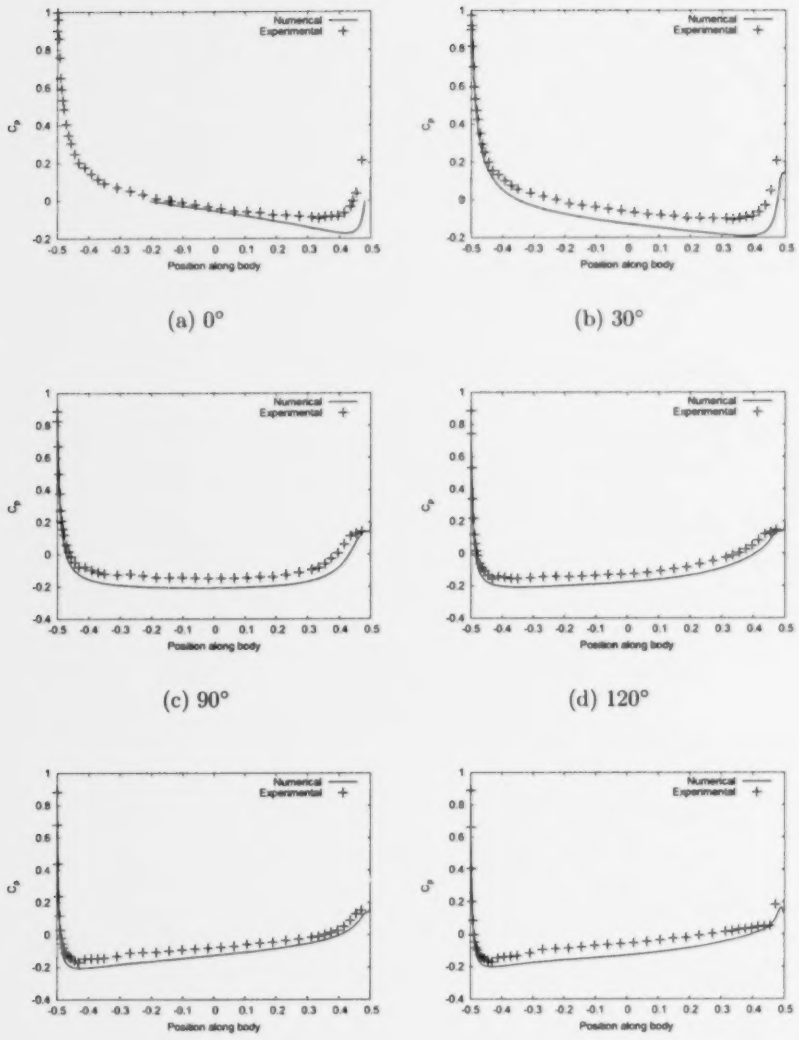

(a) 0° (b) 30°

(c) 90° (d) 120°

(e) 150° (f) 180°

Figure 11: *Pressure distribution on spheroid with extended boundary*

4.3 Hulls

During the last decade, a large number of experiments have been carried out in wind tunnels (on double-body models) and in towing tanks on various hull geometries. Many of these are appropriate for CFD validation. Stern et. al. [23] provide an excellent synopsis of the available studies. Much of the data is available on the Marnet database https://pronet.wsatkins.co.uk/marnet.

The grids used for the hulls share a common geometry. The freestream flow is parallel to the x-axis, flowing in from the negative direction. The upstream symmetry plane, the hull, and the downstream symmetry plane form the η-lo plane. The ζ-lo and ζ-hi sides form the symmetry plane below and perpendicular to the hull, respectively.

The boundary conditions used are similar for all hull cases. Inflow and outflow are applied at the ξ-lo and ξ-hi sides, respectively. Symmetry is enforced at the ζ-lo, ζ-hi, and portions of the η-lo boundary not on the hull. The farfield boundary, η-hi, uses a specified condition, with $\vec{v} = \{1, 0, 0\}$, and pressure and the turbulence quantity extrapolated from the interior.

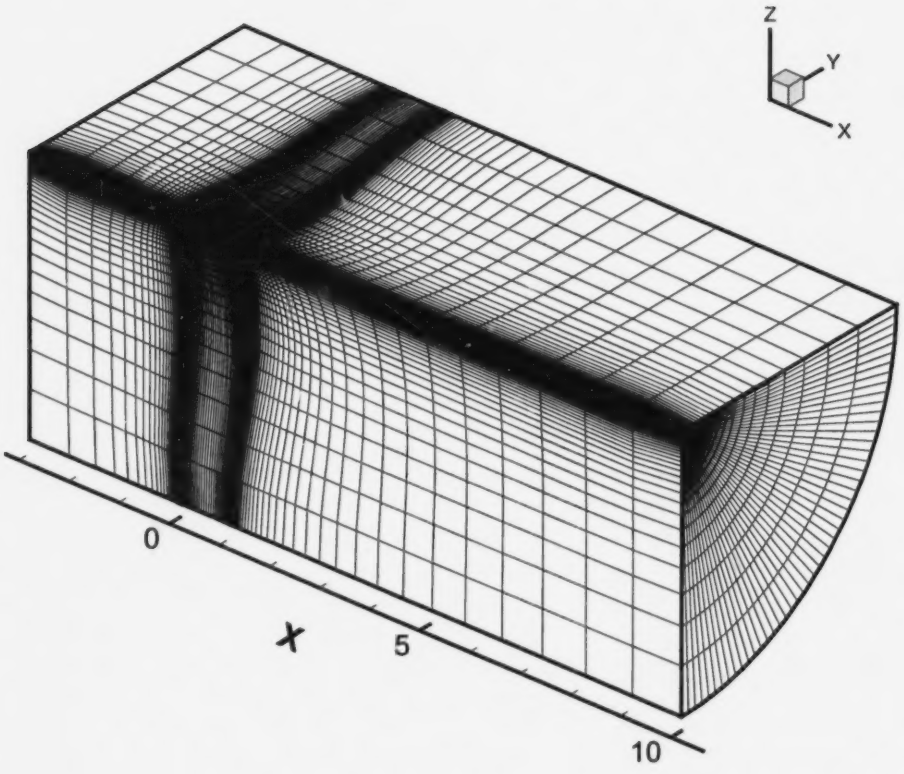

Figure 12: *Grid around Wigley hull*

4.3.1 Wigley Hull

The mathematically-defined Wigley hull has been a staple for CFD validation. However, most of the experimental data available is from towing-tanks, so that there is a free-surface condition. The only double-body type data available is a Ph.D. thesis by Sarda [24]. Unfortunately, the data is not available in electronic form (the author is now an investment banker in Tokyo). Comparisons are made against scanned copies of the results. The Reynolds number of the flow is $4.5 \cdot 10^6$.

The overall grid and grid on the body are shown in Figures 12 and 13. The grid dimensions are 118 in the streamwise direction, 80 in the off-wall direction, and 50 girthwise, giving a grid with 472,000 nodes. Note that the Wigley hull packaged with the original gem3d is not the correct shape.

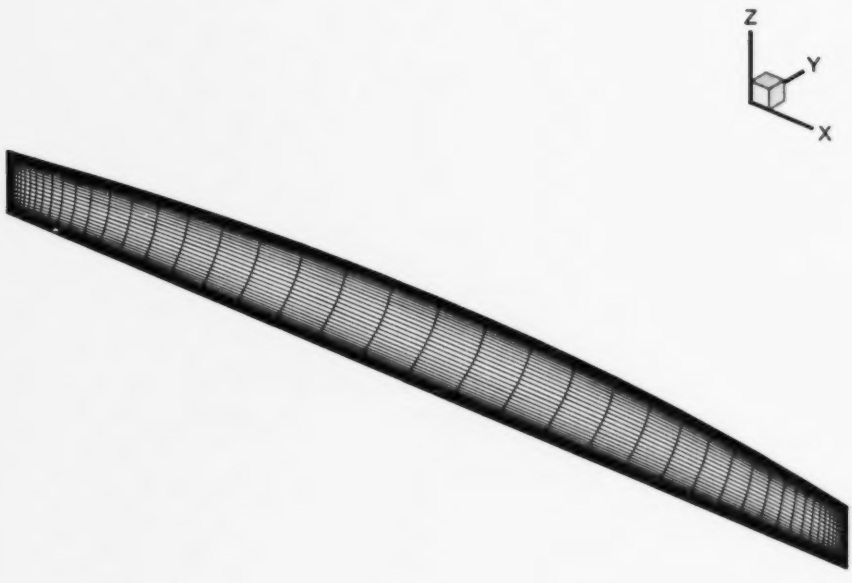

Figure 13: *Grid on body of Wigley hull*

Figures 14, 15, and 16 compare the experimental and numerical streamwise velocity profiles at 50%, 90% and 100% of the way along the hull. The boundary layer is quite similar, except at the symmetry planes, where there is an obvious error. The symmetry conditions are based on zeroth-order extrapolations. The best way to address this problem would be to increase the order of the extrapolation. Unfortunately, this destabilized the system, for reasons which are not clear. The problem occurred in both the turbulence model and the mean flow equations. A steady rise in residual was seen near the bow and stern, within a few nodes of the symmetry planes.

A second way to improve the results near the symmetry plane is to increase the grid resolution in the area. The resolution at the body should be sufficient, but rapidly deteriorates moving in the off-wall direction. The simplest, though perhaps not the most efficient, is to set the spacing at the symmetry plane on the far boundary to match that at the body. This results in highly stretched cells near the far-field, but gives good spatial resolution on the symmetry boundaries. Unfortunately, this approach causes problems with the grid generator, and it is much more difficult to get well-smoothed results. However, a decent grid was generated for the Wigley hull. Note that the grid formed has the same number of nodes. Decreasing the spacing at the symmetry plane simply pulls in nodes from the interior.

The results of using this grid are shown in Figures 17, 18, and 19. These are significantly improved. Ideally, however, the problem with the higher-order extrapolation would be addressed, easing the grid generation.

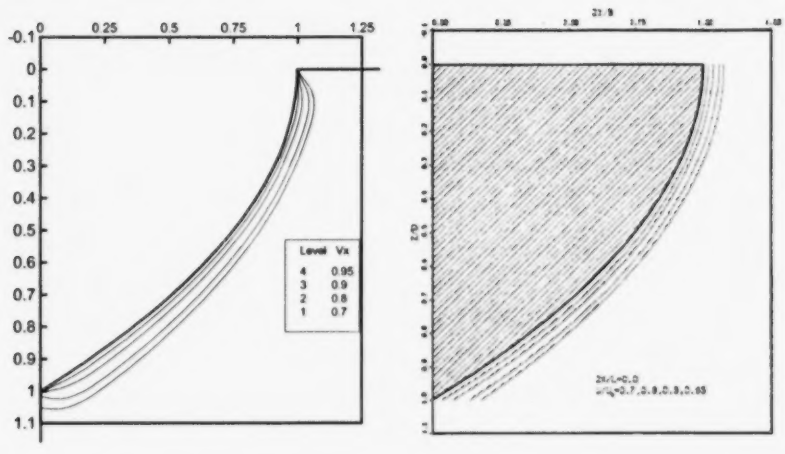

(a) Numerical (b) Experimental

Figure 14: *Streamwise velocity on Wigley hull* $x = 0.5$

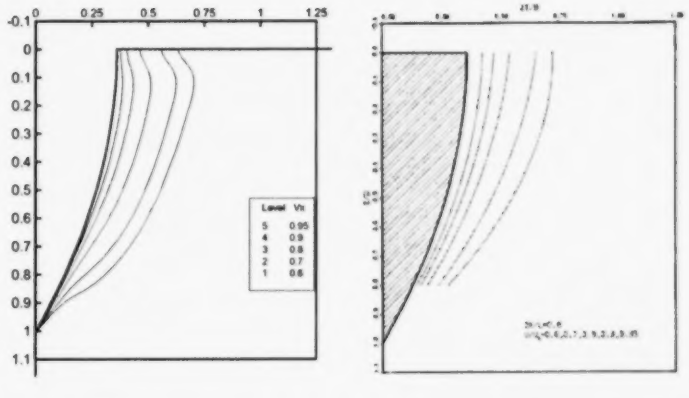

(a) Numerical (b) Experimental

Figure 15: *Streamwise velocity on Wigley hull* $x = 0.9$

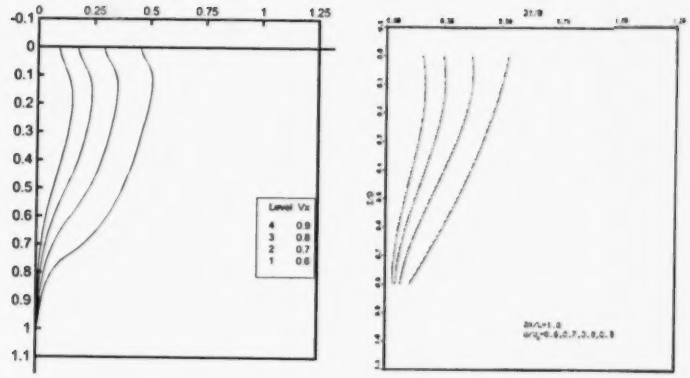

(a) Numerical (b) Experimental

Figure 16: *Streamwise velocity on Wigley hull* $x = 1.0$

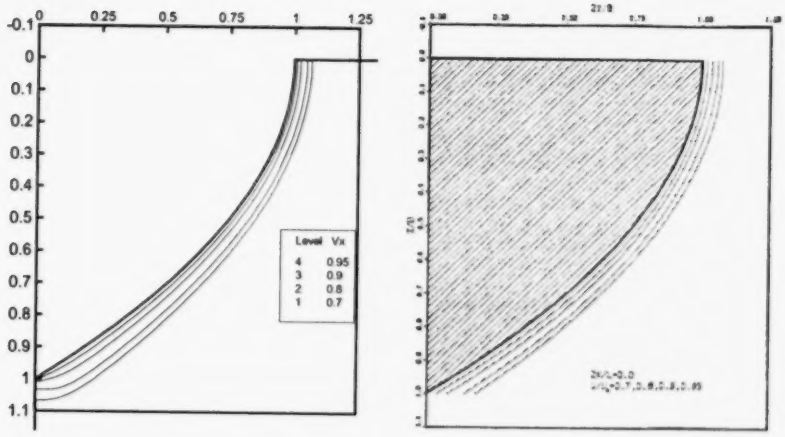

(a) Numerical (b) Experimental

Figure 17: *Streamwise velocity on Wigley hull* $x = 0.5$*, with fine symmetry*

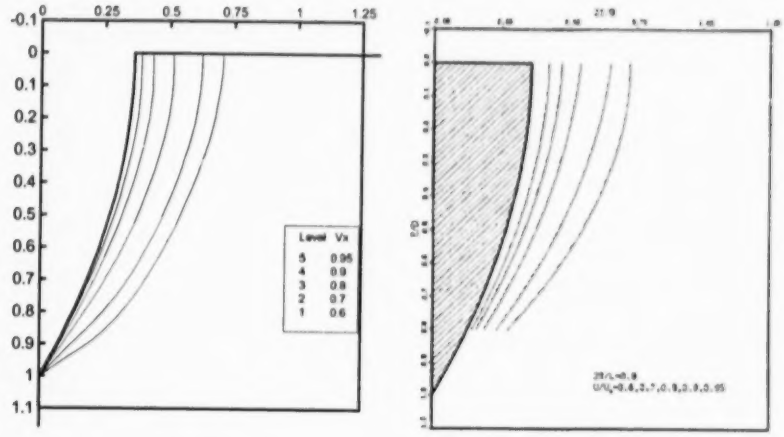

(a) Numerical (b) Experimental

Figure 18: *Streamwise velocity on Wigley hull $x = 0.9$, with fine symmetry*

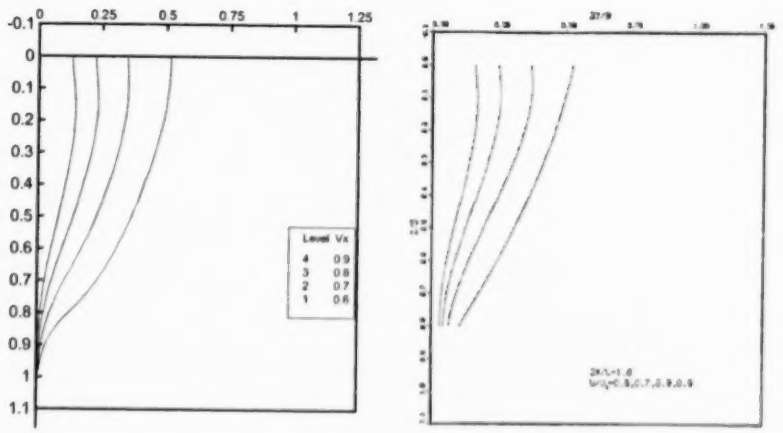

(a) Numerical (b) Experimental

Figure 19: *Streamwise velocity on Wigley hull $x = 1.0$, with fine symmetry*

4.3.2 Dyne Hull

The next hull investigated was the Dyne hull, a modification of the HSVA tanker. It was used as a 'mystery' case for CFD validation at the SSPA-CTH-IIHR workshop in 1990. Denker et. al. [25] provide wind tunnel mean velocity and turbulence measurements. The results were used in a numerical study of the effect of Reynolds number by Eca and Hoekstra [26]. This is a reasonably simple geometry, although it creates some complex flow patterns. The data set provided has both windtunnel and towing tank results. Unfortunately, the wind tunnel measurements do not include force measurements. Three-component velocities and surface pressures are available at four positions along the hull. The Reynolds number was $5 \cdot 10^6$. The flow is assumed to be fully turbulent.

Interpreting the geometry was not without difficulties. The geometry provided was for the full scale vessel, and thus includes portions of the hull above the water line. There appears to be a subtle difference between the geometries of the full scale vessel and the wind tunnel model, since the ratios of the L_{pp} to the beam and draft are somewhat different. Also, it is not clear how the L_{pp} (length between perpendiculars) is determined on the full scale vessel, as non-dimensionalized length falls midway along the 'tail' of the stern. This caused some problems with comparing the numerical results (which are necessarily based on the full scale geometry) with the wind tunnel results, which appear to have a different position for the L_{pp}. This conclusion is based on the appearance of windtunnel results slightly inside the hull of the numerical data when plotting.

Creating the grid required forming a representation of the hull. The surface is given in two parts, the main body and the tail. The reason for this is a vertical discontinuity. See Figure 20. The shape is given in a series of profiles at constant x. This form cannot be used by the surface grid generator because the discontinuity is in the same direction at the surface representation. Instead, the hull needs to be represented as a series of splines running in the streamwise direction, perpendicular to the discontinuity. To accomplish this, each of the constant x profiles were splined. Then, points along each spline were extracted and used to create a series of perpendicular splines. The original (vertical) splines were all too long since they represent a complete hull, so they needed to be cut off at the specified draft. Also, the end of the tail was problematic, due to the fact that the tail ended in between vertical splines. A single spline was created along the trailing edge of the tail. This was used to terminate each of the horizontal splines, giving a smooth representation at the trailing edge. The final grid on the hull is shown in Figure 21.

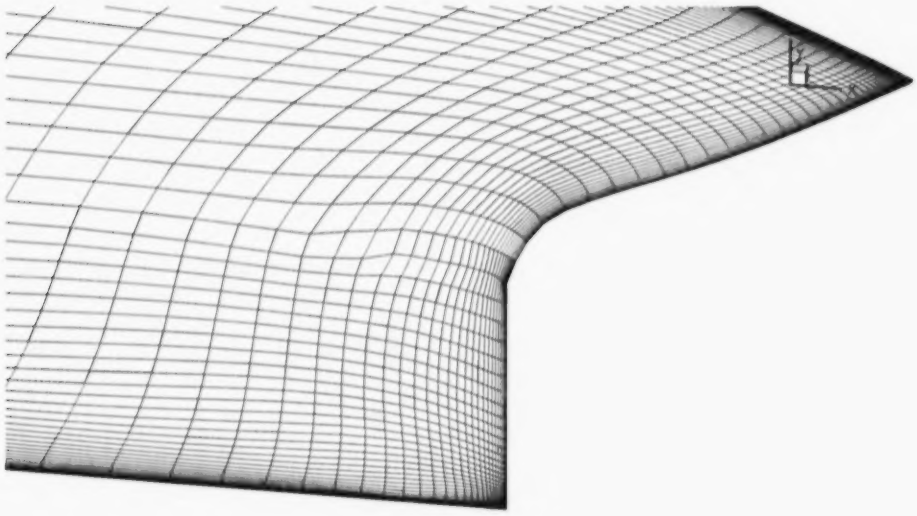

***Figure 20:** Dyne tail*

We see an effect similar to that seen at the symmetry planes of the Wigley grid, although not as obvious. The effects of refining the symmetry plane is shown in Figure 22. The following results use the refined symmetry grid.

Interpreting the experimental data was challenging. The data were reformatted with Delaunay triangulation so that they could be plotted. Figures 23 through 26 compare the streamwise velocities. The left side of the plot is the experimental data, the right the computational results. Figures 27 and 28 show the cross-flow velocities, while Figures 29 to 31 show the pressure distributions on the hull. The correlation is reasonably strong.

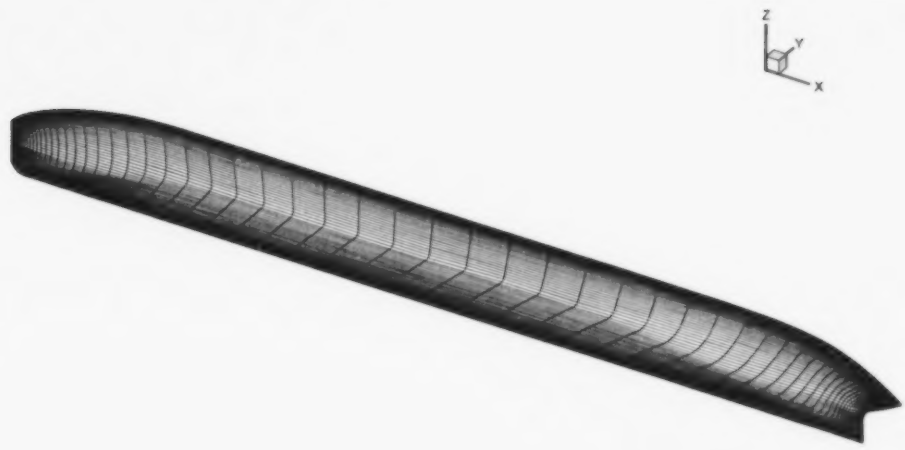

Figure 21: *Dyne hull*

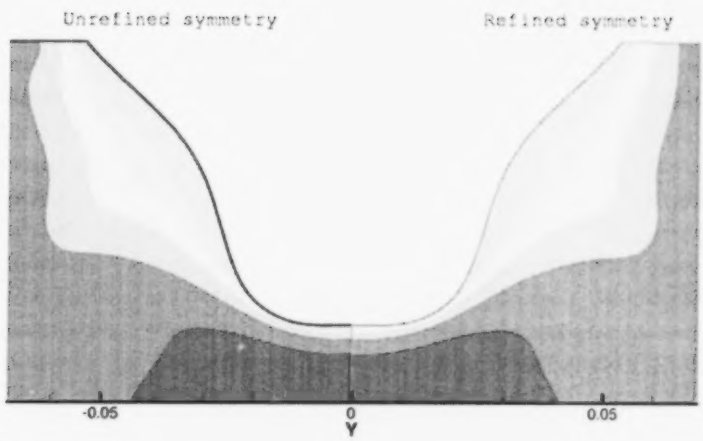

Figure 22: *Effect of refined symmetry*

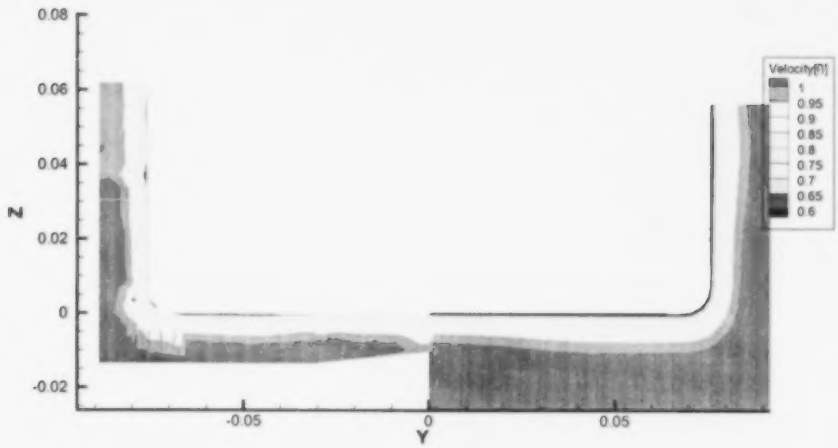

Figure 23: *Streamwise velocity on Dyne hull,* $x = 0.646$

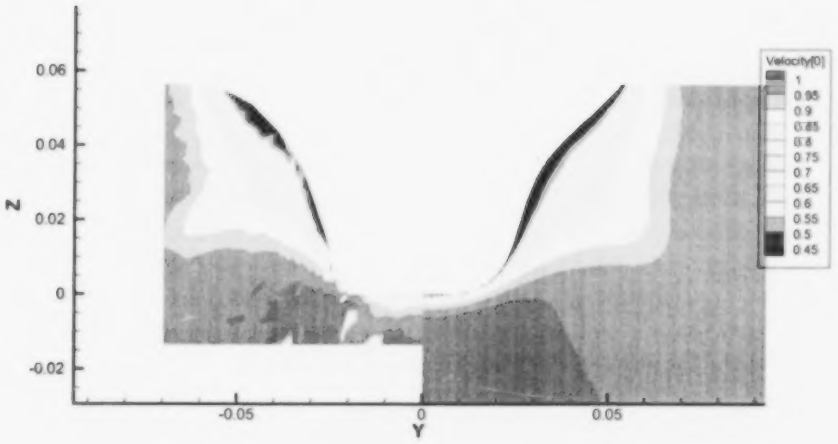

Figure 24: *Streamwise velocity on Dyne hull,* $x = 0.921$

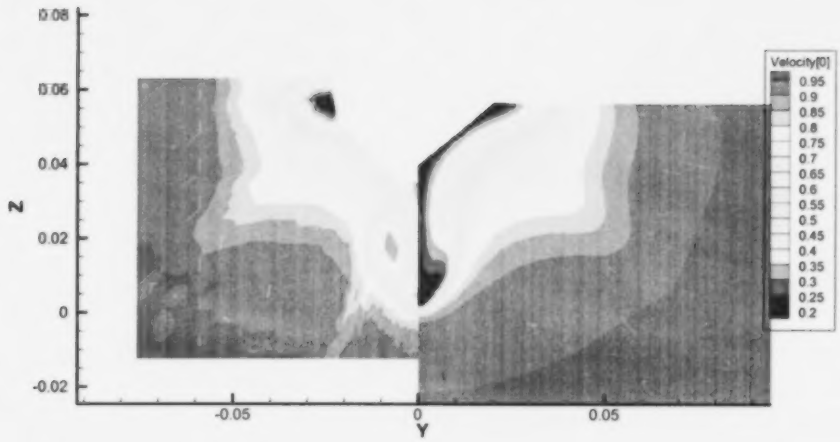

Figure 25: *Streamwise velocity on Dyne hull,* $x = 0.989$

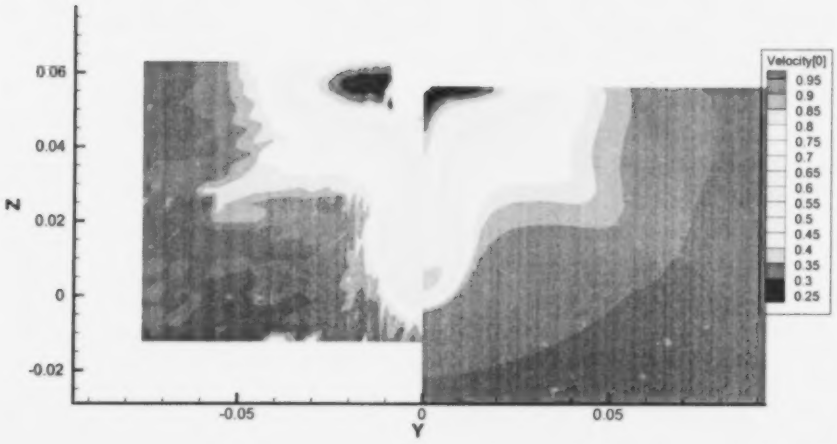

Figure 26: *Streamwise velocity on Dyne hull,* $x = 1.018$

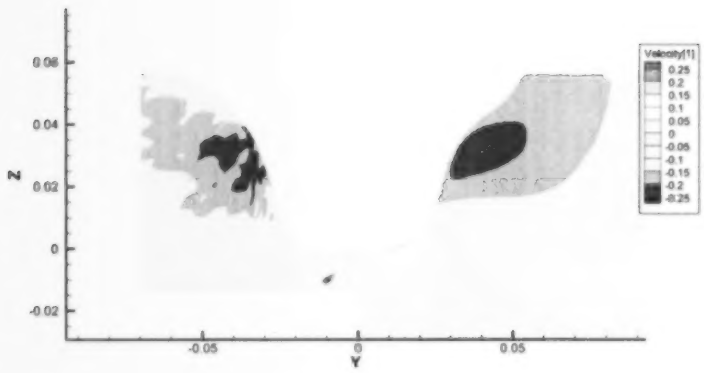

(a) V_y

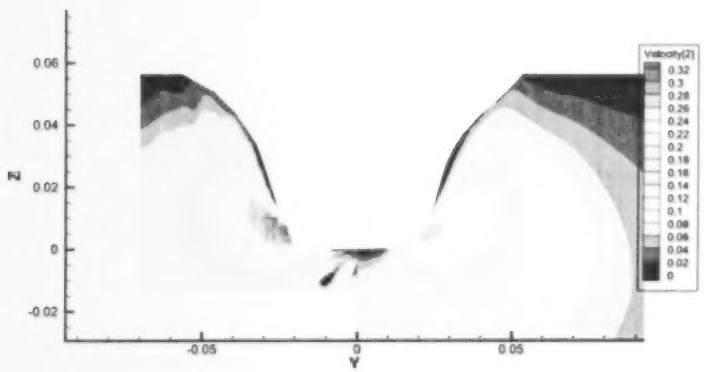

(b) V_z

Figure 27: *Cross-flow velocities on Dyne hull, x=0.921*

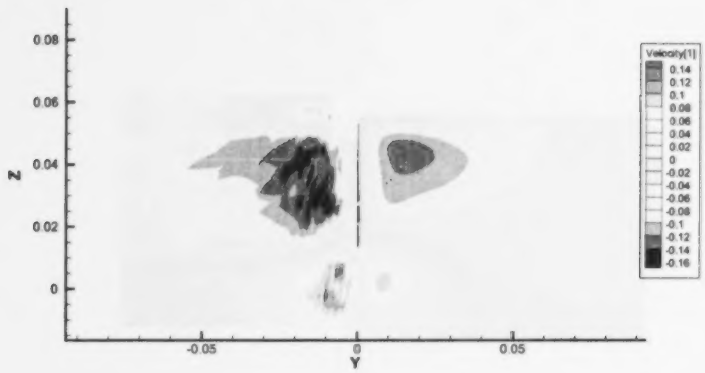

(a) V_y

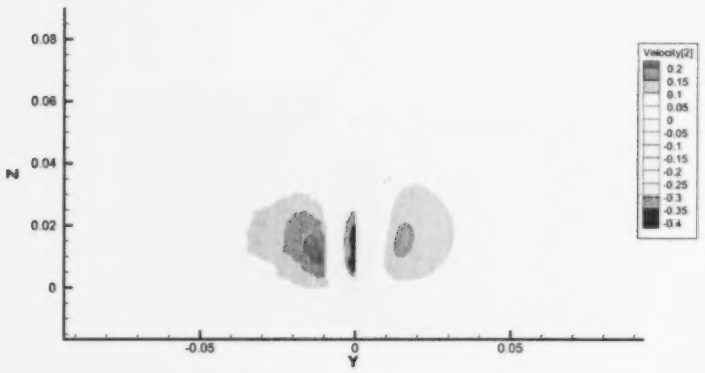

(b) V_z

Figure 28: *Cross-flow velocities on Dyne hull, x=1.018*

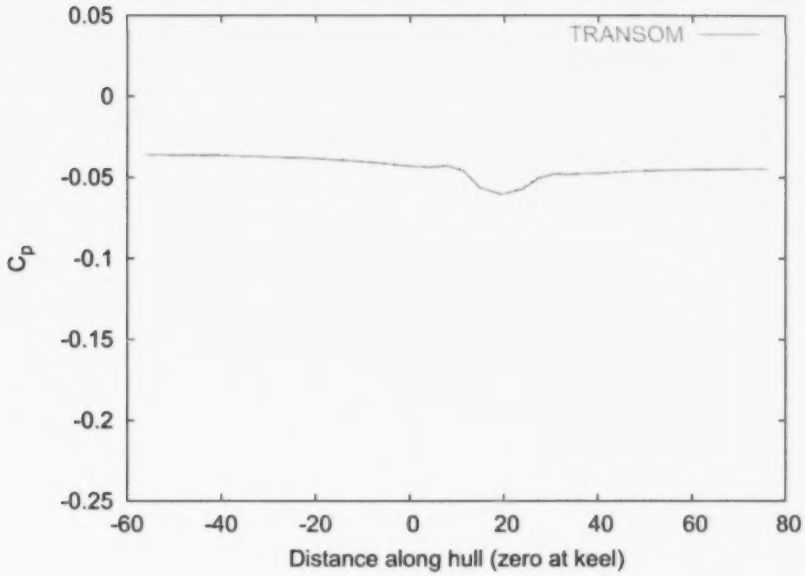

Figure 29: *Pressure on Dyne hull,* $x = 0.645$

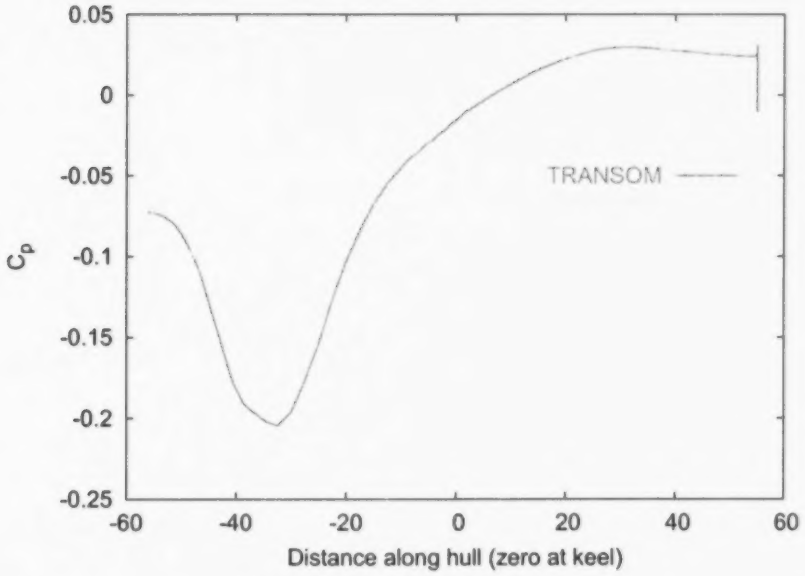

Figure 30: *Pressure on Dyne hull,* $x = 0.917$

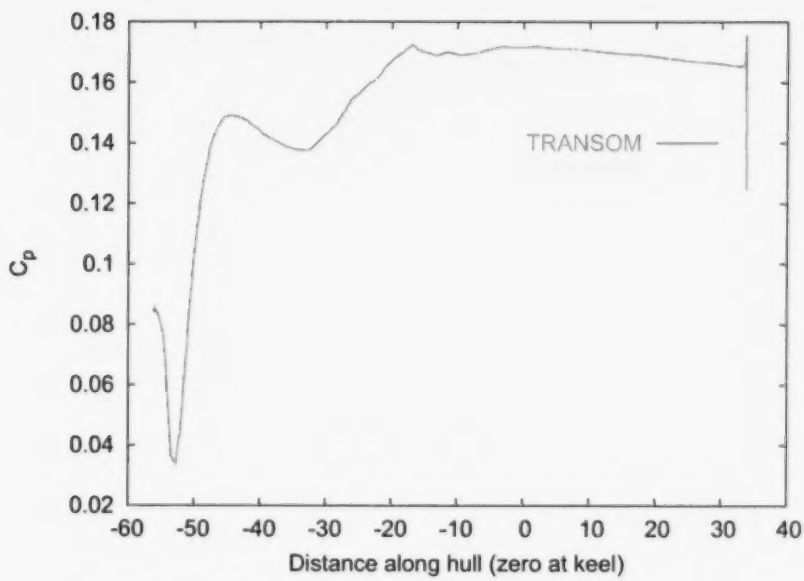

Figure 31: *Pressure on Dyne hull,* $x = 0.964$

***Figure 32:** Kriso hull*

4.3.3 Kriso KCS Hull

A more complex and modern hull is the Kriso KCS container ship. A windtunnel test was performed by Lee et. al. [27]. Free-surface data is also available. This hull, shown in Figure 32, has a bulbous bow and propeller stub. The grid generation was eased enormously because the hull surface definition was provided in grid form, as well as the more usual offset format. The grid format eliminated the process of separately generating the bow, body, and tail, then joining. The grid provided was not used directly, but instead was used to create a surface model, so that the nodes could be clustered near the bow and stern.. There are discontinuities in the grid here, where the symmetry plane meets the front of the bow. The curves of the bulbous bow, especially, make the grid generation quite difficult, as the elliptical solver tends to diverge. A grid with refined symmetry boundaries could not be successfully produced. Figures 33(a) and 33(b) show the grid around the bow and stern.

The experimental data are conveniently provided in Tecplot form. They are given in a series of slices at various stations. Unfortunately, the relationship between physical coordinates and station number was not explicitly given, so an educated guess was made. We assumed that the hull was divided into 20 stations. This assumption is based on the model length, which is two metres. Note that station zero is at the aft perpendicular, with stations increasing when moving toward the bow. The Reynolds number was $4.6 \cdot 10^6$. The flow was assumed to be fully turbulent.

Figures 34 through 38 show the velocities at each of the stations provided.

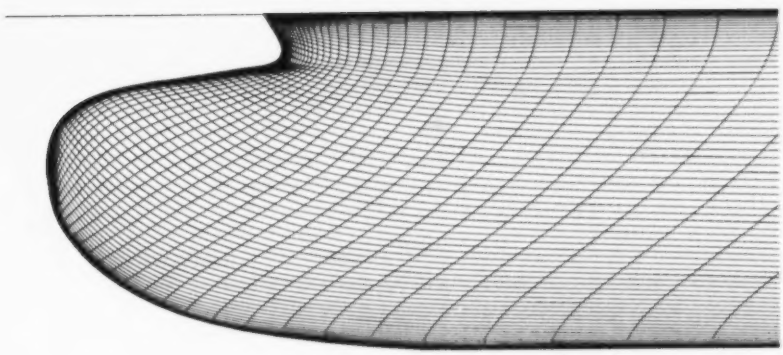

(a) Bow

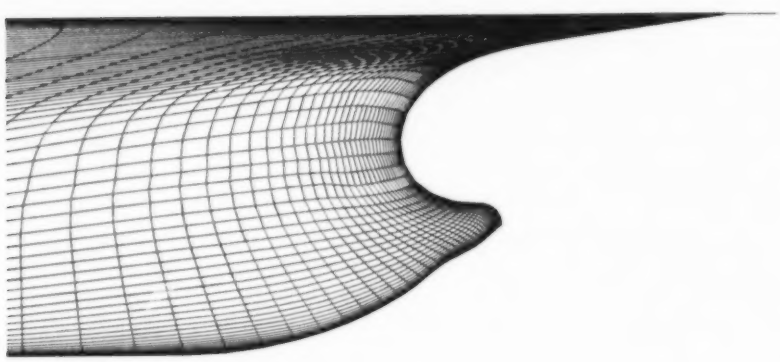

(b) Stern

Figure 33: *Kriso body grid detail*

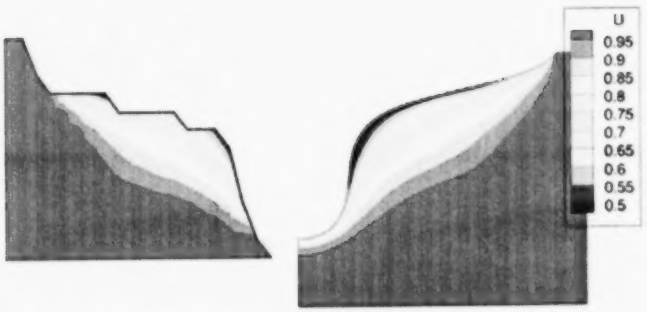

(a) V_x

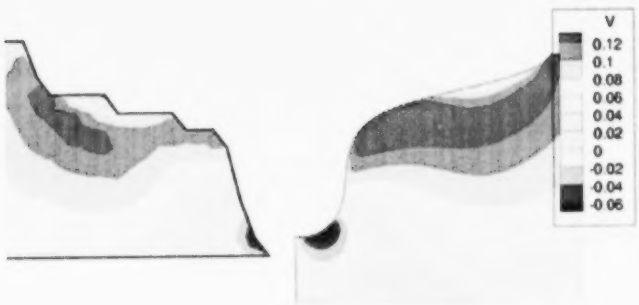

(b) V_y

(c) V_z

Figure 34: *Kriso hull velocities at station 2*

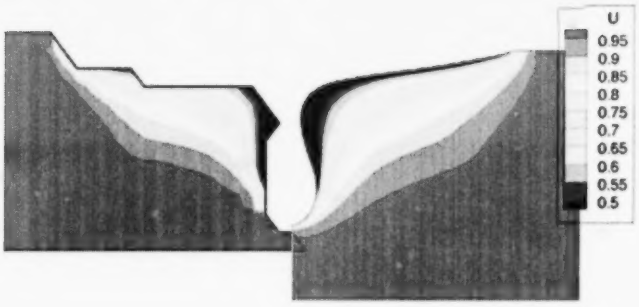

(a) V_x

(b) V_y

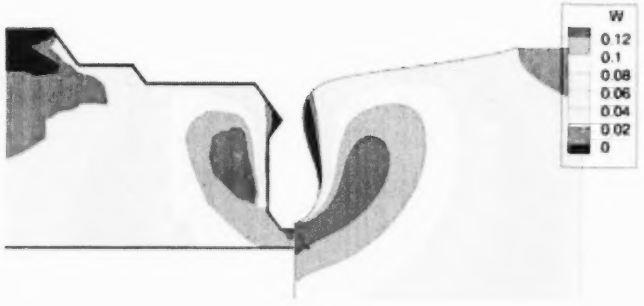

(c) V_z

Figure 35: *Kriso hull velocities at station 1*

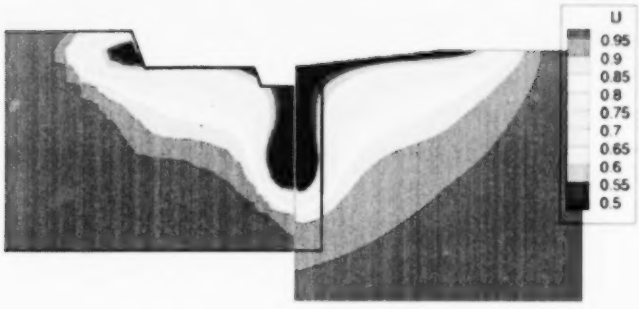

(a) V_x

(b) V_y

(c) V_z

Figure 36: *Kriso hull velocities at station 0.35*

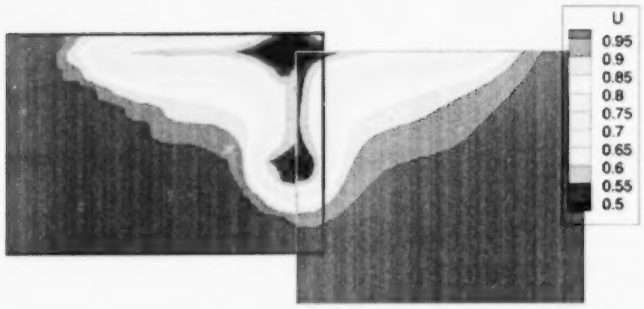

(a) V_x

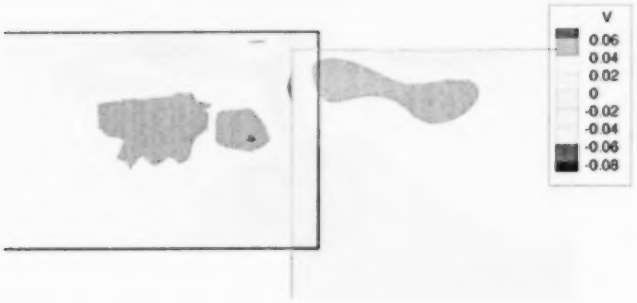

(b) V_y

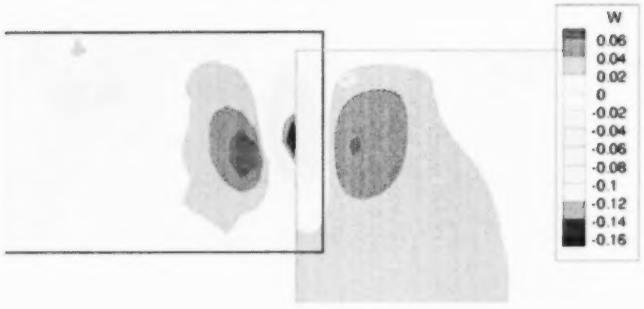

(c) V_z

Figure 37: *Kriso hull velocities at station -0.5767*

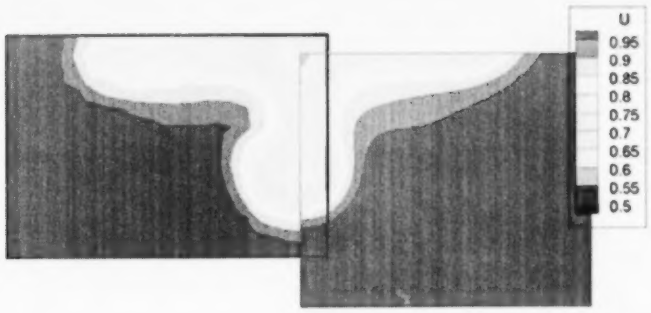

(a) V_x

(b) V_y

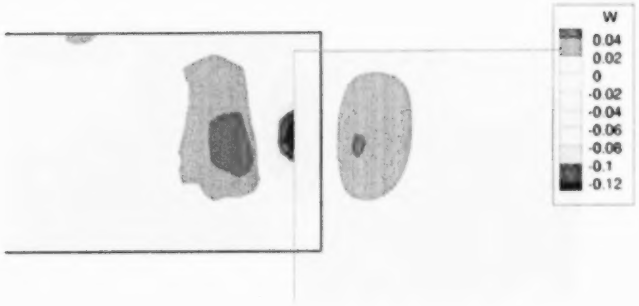

(c) V_z

Figure 38: *Kriso hull velocities at station -2*

5 Conclusions

Achieving convergence with TRANSOM relies heavily on the quality of grid used. Specifically, there must be no negative Jacobians of the curvilinear coordinate transformation. Providing these grids for even mildly complex geometries can be difficult and very time consuming. Even with what appears to be a good grid, TRANSOM can be difficult to converge. More study needs to be performed to determine the cause of this before significant effort can be expended in improving accuracy. Developing more user-friendly tools to generate grids of the required quality would also ease the process significantly.

The results achieved suggest some changes. The freestream boundary condition seems to require a very remote far-field boundary. A Riemann-type boundary condition may be more appropriate. No success was had converging with higher-order symmetry boundary conditions. Using the lower-order condition affects the accuracy noticeably. Increasing clustering at these boundaries makes grid generation even more difficult, and requires either increasing grid size or removing nodes from other areas of the grid.

The test cases given provide a solid base for further experimentation. There is clearly an error, shown by the boundary layer velocity plots from the spheroid case (see Figures 9 and 10) and pressure distribution plots (Figures 11 and 29 to 31). While some of this may be attributed to the turbulence model, grid refinement studies must be performed and the outer boundary moved even further out before this can be quantified. Note that the experimental data contain some error as well. Overall, the results show that TRANSOM is capable of providing reasonably accurate results for turbulent flows around ship hulls.

References

1. Hall, D. J., Zingg, D. W., and Ethier, C. R. (1992). An Elliptic Grid Generator for Ship Hulls. Technical Report. DRDC.

2. Hall, D. J., Zingg, D. W., and Ethier, C. R. (1993). A Laminar Incompressible Navier-Stokes Flow Solver. Technical Report. DRDC.

3. Blanco, M., Zingg, D. W., and Ethier, C. R. (1996). A Three-Dimensional Incompressible Navier-Stokes Flow Solver. Technical Report. DRDC.

4. Hall, D. J., Zingg, D. W., and Ethier, C. R. (1994). A Two-Dimensional Incompressible Navier-Stokes Turbulent Flow Solver. Technical Report. DRDC.

5. Giansante, P. D., Zingg, D. W., and Ethier, C. R. (1995). A Two-Dimensional Incompressible Navier-Stokes Turbulent Flow Solver: Code Enhancement and Convergence Acceleration. Technical Report. DRDC.

6. Hally, David (1997). TRANSOM: A Multi-Method Reynolds-Averaged Navier-Stokes Solver: Overall Design. Technical Report. DRDC.

7. Blanco, M., Chisholm, T., Zingg, D. W., and Ethier, C. R. (1997). Improvements to the NSI Incompressible Navier-Stokes Flow Solvers and Two-Dimensional Multiblock Enhancement of TRANSOM. Technical Report. DRDC.

8. Chisholm, T., Zingg, D. W., and Ethier, C. R. (1999). Further Improvements to TRANSOM. Technical Report. DRDC.

9. Chisholm, T. and Zingg, D. W. (2000). Modification of TRANSOM to Calculate Rotating Flows. Technical Report. DRDC.

10. Chorin, A. J. (1968). Numerical Solution of the Navier-Stokes equations. *Math. Comp.*, Vol. 22.

11. Kwak, D. (1989). Computation of viscous incompressible flows. Technical Report. Lecture Notes for the Von Karman Institute for Fluid Dynamics Lecture Series: Computational Fluid Dynamics.

12. Rogers, S. E., Kwak, D., and Kiris, C. (1991). Steady and unsteady solutions of the incompressible Navier-Stokes equations. *AIAA Journal*, Vol. 29.

13. Rogers, S. E. and Kwak, D. (1988). An upwind differencing scheme for the incompressible Navier-Stokes equations. (Technical Report Tech. Rep. TM-101051). NASA.

14. Rogers, S. E. (1995). A comparison of implicit schemes for the incompressible Navier-Stokes equations with artificial compressibility. (Technical Report Tech. Rep. 95-0567). AIAA.

15. Saad, Y. and Schultz, M. H. (1986). GMRES: a generalized minimum residual algorithm for solving nonsymmetric linear systems. *SIAM J. Sci. Stat. Computing*, **7**, 856–869.

16. Spalart, P. and Allmaras, S. (1992). A One-Equation Turbulence Model for Aerodynamic Flows. AIAA paper 92-0439.

17. Chisholm, T. and Zingg, D. W. (2003). Start-up Issues in a Newton-Krylov Algorithm for Turbulent Aerodynamic Flows. AIAA paper 03-3708.

18. Chesnakas, C. J. and Simpson, R. L. (1996). Measurements of the Turbulence Structure in the Vicinity of a 3-D Separation. *Journal of Fluids Engineering*, **118**(1).

19. Chesnakas, C. J. and Simpson, R. L. (1997). A Detailed Investigation of the 3-D Separation about a 6:1 Prolate Spheroid at Angle of Attack. *AIAA Journal*, **35**(6).

20. Wetzel, T. G. (1996). Unsteady Flow Over a 6:1 Prolate Spheroid. Ph.D. thesis. Dept. of Aero and Ocean Engr, VPI and SU.

21. Kreplin, H. P. (1994). Three dimensional boundary layer and flow field data of an inclined prolate spheroid. In *A Selection of Experimental Test Cases for the Validation of CFD Codes*, Number 303, AGARD.

22. Constantinescu, G. S., Pasinato, H., Wang, Y. Q., and Squires, K. D. (2002). Numerical investigation of flow past a prolate spheroid. (Technical Report Tech. Rep. 2002-0588). AIAA.

23. Stern, F., Longo, J., Abdel-Maksoud, M., and Suzuki, T. (1998). Evaluation of Surface-Ship Resistance and Propulsion Model-Scale Database for CFD Validation. In *Proceedings of the 1st Symposium on Marine Applicaton of Computational Fluid Dynamics.*

24. Sarda, Om P. (1986). Turbulent Flow Past Ship Hulls - An Experimental and Computational Study. Ph.D. thesis. University of Iowa.

25. J., Denker, T., Knaack, and J., Kux (1992). Experimental and numerical investigations of the HSVA-tanker-2 flow field. Technical Report. Institute of Shipbuilding (IfS) Rept. 521.

26. Eca, L. and Hoekstra, M. (1997). Numerical Calculations of Ship Stern Flows at Full-Scale Reynolds Numbers. Twenty-First Symposium on Naval Hydrodynamics.

27. Lee, Sang-Joon, Kim, Hak-Rok, Kim, Wu-Joan, and Van, Suak-Ho (2003). Wind tunnel tests on flow characteristics of the KRISO 3600 TEU containership and 300K VLCC double-deck ship models. *Journal of Ship Research*, **47**(1).

Distribution List

CANADA

Internal

1 Scientific Authority

5 Library

Department of National Defence

National Defence Headquarters
MGen. George R. Pearkes Bldg.
101 Colonel By Drive
Ottawa, Ontario
K1A OK2

1 DRDCIM

2 DMSS 2

Others

2 Authors

2 Canada Institute for Scientific and Technical Information
Library Serials Acquisitions
National Research Council Canada
Ottawa, Ontario
K1A OS2

2 Canadian Acquisitions Division
National Library of Canada
395 Wellington Street
Ottawa, Ontario
K1A ON4
Attn: Government Documents

1 Director-General
Institute for Marine Dynamics
National Research Council of Canada
P.O. Box 12093, Station A
St. John's, Newfoundland
A1B 3T5

1 Director-General
Institute for Aerospace Research
National Research Council of Canada
Building M-13A
Ottawa, Ontario
K1A OR6

1 Transport Development Centre
Transport Canada
6th Floor
800 Rene Levesque Blvd, West
Montreal, Que.
H3B 1X9
Attn: Marine R&D Coordinator

1 Canadian Coast Guard
Ship Safety Branch
Canada Building, 11th Floor
344 Slater Street
Ottawa, Ontario
K1A 0N7
Att: Chief, Design and Construction

MOUs

15 Canadian Project Officer ABCA-02-01 (C/SCI, DRDC Atlantic – paper copies only)

DOCUMENT CONTROL DATA

(Security classification of title, body of abstract and indexing annotation must be entered when document is classified)

1. ORIGINATOR (the name and address of the organization preparing the document. Organizations for whom the document was prepared, e.g. Centre sponsoring a contractor's report, or tasking agency, are entered in section 8.)

University of Toronto, Institute of Aerospace Studies
4925 Dufferin St., Toronto, ON, M3H 5T6

2. SECURITY CLASSIFICATION (overall security classification of the document including special warning terms if applicable).

UNCLASSIFIED

3. TITLE (the complete document title as indicated on the title page. Its classification should be indicated by the appropriate abbreviation (S,C,R or U) in parentheses after the title).

Validation of TRANSOM

4. AUTHORS (Last name, first name, middle initial. If military, show rank, e.g. Doe, Maj. John E.)

Chisholm, T. ; Zingg, D.W.

5. DATE OF PUBLICATION (month and year of publication of document)	6a. NO. OF PAGES (total containing information. Include Annexes, Appendices, etc).	6b. NO. OF REFS (total cited in document)
October 2004	53	27

7. DESCRIPTIVE NOTES (the category of the document, e.g. technical report, technical note or memorandum. If appropriate, enter the type of report, e.g. interim, progress, summary, annual or final. Give the inclusive dates when a specific reporting period is covered).

Contractor Report

8. SPONSORING ACTIVITY (the name of the department project office or laboratory sponsoring the research and development. Include address).

Defence R&D Canada – Atlantic
PO Box 1012, Dartmouth, NS, Canada B2Y 3Z7

9a. PROJECT OR GRANT NO. (if appropriate, the applicable research and development project or grant number under which the document was written. Specify whether project or grant).	9b. CONTRACT NO. (if appropriate, the applicable number under which the document was written).
Project 11cj18	W7707-1-1110

10a. ORIGINATOR'S DOCUMENT NUMBER (the official document number by which the document is identified by the originating activity. This number must be unique.)	10b. OTHER DOCUMENT NOs. (Any other numbers which may be assigned this document either by the originator or by the sponsor.)
DRDC Atlantic CR 2004-229	

11. DOCUMENT AVAILABILITY (any limitations on further dissemination of the document, other than those imposed by security classification)

(X) Unlimited distribution
( ) Defence departments and defence contractors; further distribution only as approved
( ) Defence departments and Canadian defence contractors; further distribution only as approved
( ) Government departments and agencies; further distribution only as approved
( ) Defence departments; further distribution only as approved
( ) Other (please specify):

12. DOCUMENT ANNOUNCEMENT (any limitation to the bibliographic announcement of this document. This will normally correspond to the Document Availability (11). However, where further distribution beyond the audience specified in (11) is possible, a wider announcement audience may be selected).

13. ABSTRACT (a brief and factual summary of the document. It may also appear elsewhere in the body of the document itself. It is highly desirable that the abstract of classified documents be unclassified. Each paragraph of the abstract shall begin with an indication of the security classification of the information in the paragraph (unless the document itself is unclassified) represented as (S), (C), (R), or (U). It is not necessary to include here abstracts in both official languages unless the text is bilingual).

A series of test cases, including a two-dimensional airfoil, flow over a prolate spheroid, and the Wigley, Dyne, and Kriso hulls, was used to validate TRANSOM, a flow solver developed at DRDC Atlantic. TRANSOM is quite sensitive to the quality of the grid. Suitable grids can be difficult to produce with the tools available. The results suggest changes to the boundary conditions to improve accuracy without requiring further restrictions on grid generation. Accurate results are obtained for most of the test cases.

14. KEYWORDS, DESCRIPTORS or IDENTIFIERS (technically meaningful terms or short phrases that characterize a document and could be helpful in cataloguing the document. They should be selected so that no security classification is required. Identifiers, such as equipment model designation, trade name, military project code name, geographic location may also be included. If possible keywords should be selected from a published thesaurus. e.g. Thesaurus of Engineering and Scientific Terms (TEST) and that thesaurus-identified. If it not possible to select indexing terms which are Unclassified, the classification of each should be indicated as with the title).

Computational fluid dynamics
Fluid flow
Ship hulls
Turbulence
Spalart-Allmaras turbulence model
TRANSOM
Wigley hull
Dyne hull
Kriso hull

Defence R&D Canada

Canada's leader in defence
and National Security
Science and Technology

R & D pour la défense Canada

Chef de file au Canada en matière
de science et de technologie pour
la défense et la sécurité nationale

www.drdc-rddc.gc.ca